Research Article

Zhihao Liao and Zhiwei Liao*

Slope stability evaluation using backpropagation neural networks and multivariate adaptive regression splines

Abstract: Slope stability assessment is a critical concern in construction projects. This study explores the use of multivariate adaptive regression splines (MARS) to capture the intrinsic nonlinear and multidimensional relationship among the parameters that are associated with the evaluation of slope stability. A comparative study of machine learning solutions for slope stability assessment that relied on backpropagation neural network (BPNN) and MARS was conducted. One data set with actual slope collapse events was utilized for model development and to compare the performance of BPNN and MARS. Research results suggest that BPNN and MARS models can model the relationship between the safety factor and the slope parameters. Also, the MARS model has the advantages of computational efficiency and easy interpretation.

Keywords: multivariate adaptive regression splines, backpropagation neural network, slope stability, safety factor

1 Introduction

Landslide is a common type of geological disaster, which always impose heavy social and economic losses [1–3]. These hazards are often caused by various uncertainties, including external factors (e.g., rainfall, earthquake, excavation) and the hydrogeological conditions of the slope [4–6].

---
* Corresponding author: Zhiwei Liao, State Key Laboratory of Coal Mine Disaster Dynamics and Control, School of Resources and Safety Engineering, Chongqing University, Chongqing, 400044, People's Republic of China, e-mail: zwliao16@cqu.edu.cn
Zhihao Liao: Construction Engineering Quality & Safety Supervision Station, Tongxiang Housing and Urban-Rural Planning and Construction Bureau, Tongxiang, Zhejiang, 314500, People's Republic of China, e-mail: 40488674@qq.com

Thus, analyzing the stability of the slope and preventing or mitigating the damage became an urgent issue for engineers and researchers. By convention, the safety factor is considered as an important index for slope stability analysis and a choice of treatment designs. The limit equilibrium method (LEM) and numerical calculation method based on the theory of elasticity and plasticity are widely used to calculate the safety factor [7–9]. However, the accuracy of the LEM is commonly affected to some extent because of the assumption on slip surface and interslice forces. Also, the numerical calculation method based on the theory of elasticity and plasticity requires the selection of a well-fitted constitutive model that can reflect the mechanical behavior of soil and rocks in slopes accurately, which is a difficult task for engineers and researchers [10–13]. Moreover, the interactions among the factors that affect slope stability are complex and multifactorial, thereby resulting in the difficult evaluation of the real slope stability based on safety factors.

In recent years, for the intrinsic capability of mining valuable information hidden in records of real slope cases, machine learning algorithms, such as artificial neural network (ANN)-based [14–19], discriminant analysis-based [20–22], and decision tree-based approaches [23–25], have been applied to the evaluation of slope stability gradually. According to the potential failure mechanism, these methods evaluate slope stability based on the characteristics of the parameters, such as geotechnical parameters, slope geometry, and water condition, and the application of these machine learning algorithms can obtain reasonable results that can be used for the evaluation of slope stability. Furthermore, even a small increment of the prediction accuracy could have a significant influence on the evaluation of slope stability [26]. Therefore, exploring high-performance-based models, which are used to predict slope stability accurately, is necessary.

This study explores the use of multivariate adaptive regression splines (MARS) [27] to capture the intrinsic nonlinear and multidimensional relationship associated with the evaluation of slope stability. A comparative study of machine learning solutions for slope stability

assessment that relied on backpropagation neural network (BPNN) and MARS was conducted. One data set with actual slope collapse events was utilized for model development and to compare the performance of BPNN and MARS.

2 BPNN

ANN is a computational model based on the structure and functions of biological neural networks that can be used to model the complex relationships between inputs and outputs or as pattern classifiers [28]. The ANN structure consists of one or more layers of interconnected neurons or nodes. Each link that connects each neuron has an associated weight. They can learn some target values (desired output) from a set of selected input data through a computing network system under supervised and self-adjusted or unsupervised learning algorithms [29]. The learning process is achieved by adjusting the weights in the network until a particular input leads to a specific target output. The predictive power of the trained neural networks can be tested by comparing the predicted value using a target.

Various algorithms for ANN have been proposed in previous literature, among which the BPNN model is the most widely used [30,31]. The network has an enhanced functionality of highly nonlinear correspondent relations that analyze input and output and fine feasibility. The BPNNs generally consist of one input layer, one or more hidden layers, and one output layer. The layers are completely connected, and each interconnection is assigned with an associative weight (Figure 1). BPNN training consists of two phases of computation: a forward pass and a backward pass. The steps in the BPNN algorithm are described as follows: first, the network weights are initialized, and the input data are presented forward from the input to the output layer, thereby producing actual output. Second, the output is compared with the target values, and an error is determined. Finally, the errors are propagated backward from the output layer to the previous layers, and the connection weights are updated to minimize the errors.

Although the number of hidden neurons is typically determined through a trial-and-error process, the number of input neurons is the same as the number of the selected factors. Normally, the smallest number of neurons that yields satisfactory results (judged by the network performance in terms of the coefficient of determination R^2 of the testing data set) is selected. In the present study, a MATLAB-based BPNN with Levenberg–Marquardt (LM) algorithm [32] was adopted for neural network modeling.
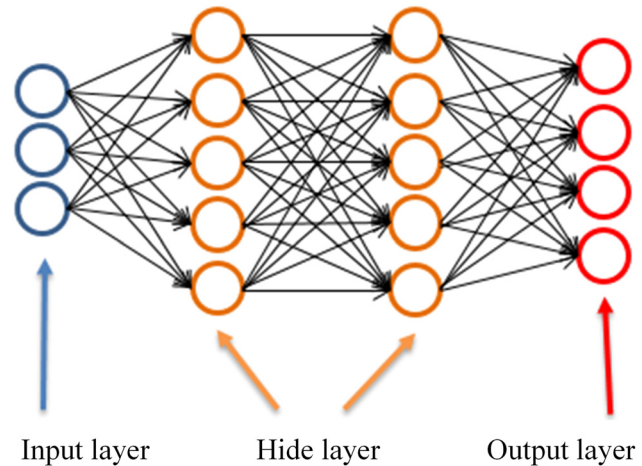

Figure 1: BPNN architecture (adapted from ref. [33]).

3 MARS

MARS is a form of regression analysis introduced by ref. [27]. This algorithm generates flexible regression models, where the nonlinear relationship between a group of input variables and their dependent outputs is approximated. MARS is a nonparametric statistical method based on a divide-and-conquer strategy, in which the training data sets are partitioned into separate piecewise linear segments (splines) of differing gradients. No restrictive assumption is made regarding the functional relationship between the dependent and independent variables in MARS. Instead, the MARS model constructs this relation from a set of coefficients and basis functions (BFs) that are entirely "driven" from the data [34].

The MARS approximation function $\hat{f}(X)$, which is a linear combination of BFs and their interactions, is expressed as follows:

$$\hat{f}(X) = a_0 + \sum_{m=1}^{M} a_m B_m(X), \tag{1}$$

where $\hat{f}(X)$ is the MARS predictor, $X = (x_1, x_2, ..., x_p)$ is the vector of the input variables, a_0 is a constant coefficient, a_m is the coefficient of the mth term, which is obtained by the least-squares method, and $B_m(X)$ is the mth BF. The MARS approximation function can be a spline function or interaction BFs produced by multiplying an existing term with a truncated linear function that involves a new/different variable. $B_m(X)$ can be a single spline BF (SBF) and the product of two or more SBFs. Thus, MARS can approximate highly nonlinear problems.

The MARS model has executed in two phases of computation: a forward phase and a backward phase. First,

the MARS model is described by only using one input variable. Candidate knots are placed at random positions within the range of each predictor to define a pair of basic functions. At each step, the knot and its corresponding pair of basic functions are fitted to yield the maximum

reduction in sum-of-squares residual error. New BFs are added until the maximum complexity or threshold value is achieved. The forward phase selection of the BF results in an extremely complex and over-fitted model.

MARS modeling is a data-driven process. To construct the model in equation (1), the forward phase is performed on the training data starting initially with only the intercept a_0. At each subsequent step, the basis pair that produces the maximum reduction in the training error is added. Considering a current model with M BFs, the next model would be updated after two BFs are added as follows:

$$\hat{f}(X) = a_0 + \sum_{m=1}^{M} a_m B_m(X) + a_{M+1}B_l(X)\max(0, x_j - t) \\ + a_{M+2}B_l(X)\max(0, t - x_j). \tag{2}$$

Even if this resulted function fits the training data well, it has a poor predictive capacity for the new data

Table 1: Detail statistical description of the data set

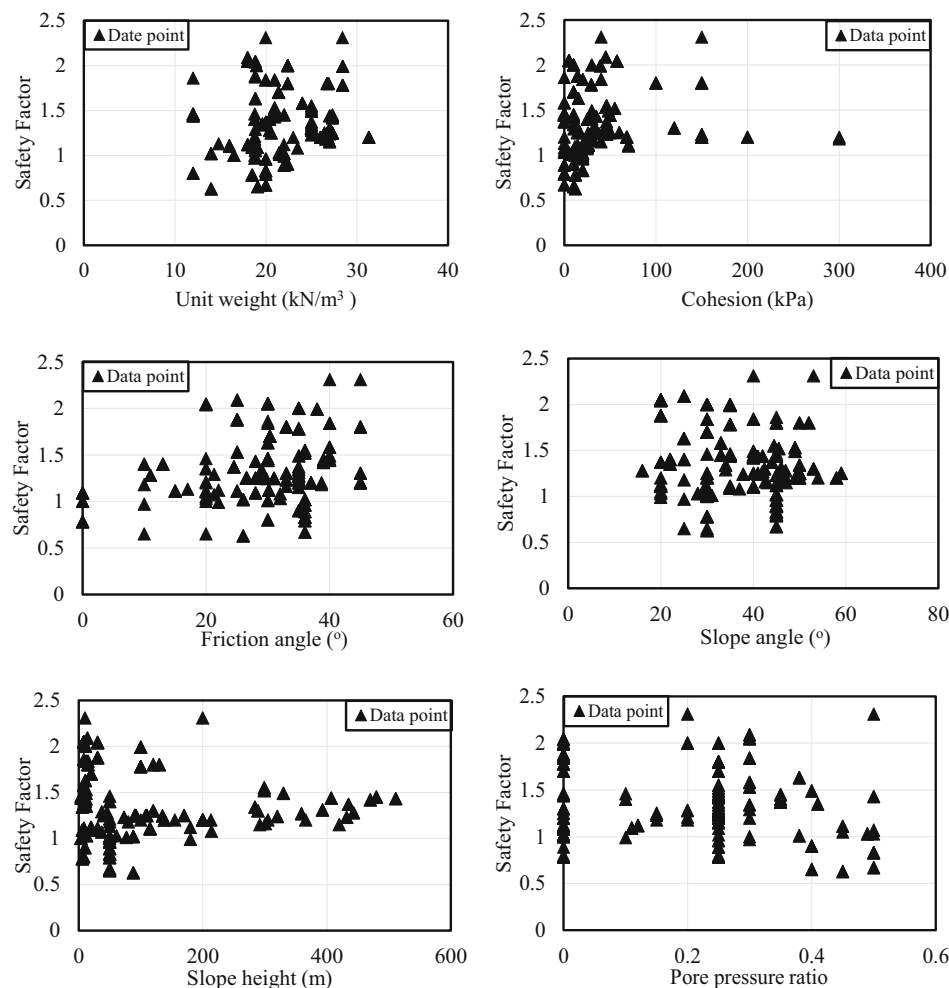| Factors	Max	Min	Average	Std	Median
Bulk weight (γ/kN/m^3)	31.30	12.00	21.76	4.13	20.96
Cohesion (c/kPa)	300.00	0.00	34.12	45.82	19.96
Friction angle (α/°)	45.00	0.00	28.73	10.58	30.24
Slope angle (β/°)	59.00	16.00	36.10	10.22	35.00
Slope height (H/m)	511.00	3.60	104.19	132.68	50.00
Pore pressure ratio (Ru)	45.00	0.00	0.48	3.45	0.25

Figure 2: Scatterplots of all influencing factors with safety factors.

set. To enhance the prediction capacity of the MARS model, the backward phase considers the residual error and the model complexity, and the redundant BFs that have the least contributions are deleted. Model subsets are compared using the less computationally expensive method of generalized cross-validation (GCV). The GCV is the mean-squared residual error divided by a penalty that is dependent on model complexity. For a training data set with N points, GCV is calculated as follows:

$$\text{GCV} = \frac{\frac{1}{N}\sum_{i=1}^{N}[y_i - \hat{f}(X_i)]^2}{\left[1 - \frac{M + d \times (M-1)/2}{N}\right]^2}, \tag{3}$$

where M is the number of BFs, y_i is the true value at X_i, $\hat{f}(X_i)$ is the predictive value at X_i, and d is a penalty for each BF included in the developed submodel. The GCV penalizes not only the number of BFs but also the number of knots.

4 History data of slopes

To explore the application of MARS in the evaluation of slope stability and compare the result with BPNN, one history data set of the slope is employed in this study. The data set contains 153 history cases that are collected from previous research [35–39]. All the 153 data samples used for further analyses are shown in the Appendix. Based on a previous study, six influencing factors are used in this data set to present the character of the slope. The factors that influence slope stability, including unit weight (γ), cohesion (c), internal friction angle (α), slope angle (β), slope height (H), and pore pressure ratio (Ru), are used to characterize the earth slope.

Table 1 shows the details of the statistical descriptions of the data set used in this study. For better recognition of the relationships between safety factors and other parameters, the scatterplots of all influencing factors with safety factors are plotted in Figure 2. The corresponding relationships between influencing factors and the safety factor were not obvious.

5 Experimental results

In this study, 80% of the data is used as training data; the rest is used to test the machine learning model. To reduce the subjectivity in the selection of training and testing data, every group of data sets is selected randomly.

In the case of BPNN, the sigmoid function is used as the action function. The number of neurons in the hidden layer is selected based on trial. In this study, the number of neurons, which ensures BPNN has excellent performance, is six. A total of 122 data, which are employed to construct the machine learning model, are included in data set 1. Moreover, six parameters should be inputted, and one output result should be generated.

To construct a MARS model, the data are packed the same way as the BPNN model. The number of basic functions, as well as the parameters associated with each one (product degree and knot locations), are automatically determined by the data. The prediction of safety factors using the MARS model with second order interaction adopted 25 BFs of linear spline function. An open MARS source code from ref. [40] is adapted to perform the analyses presented in this study.

5.1 Prediction of the safety factor

Figure 3 shows the comparison of predicted safety factor and target value in slopes based on the BPNN
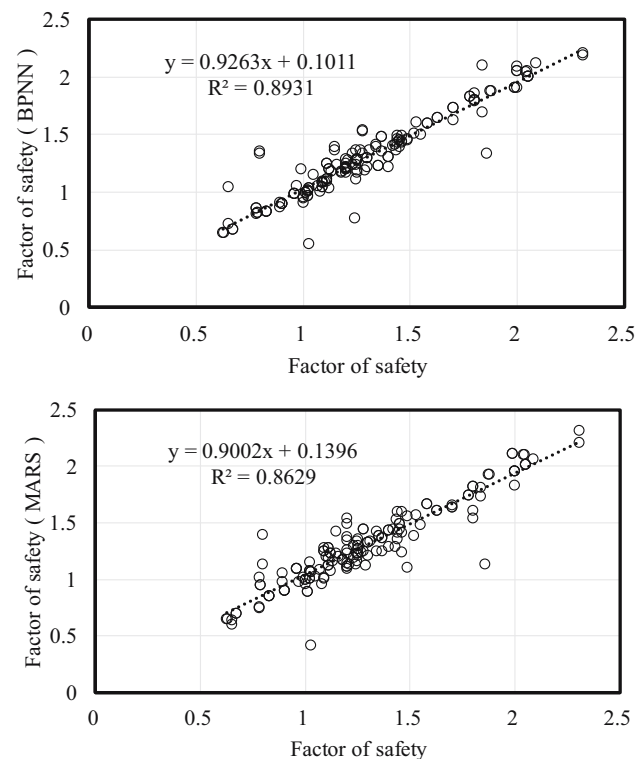

Figure 3: Comparison of predicted safety factor and target value in slopes.

Table 2: ANOVA decomposition for the MARS model

Func.	STD	GCV	Basis	Params.	Variable (s)
1	0.5	2.208	1	2.5	Slope angle (β)
2	0.329	0.829	1	2.5	Slope height (H)
3	0.065	0.071	1	2.5	Pore pressure ratio (Ru)
4	0.081	0.085	1	2.5	Bulk weight (γ), cohesion (kPa)
5	0.216	0.319	1	2.5	Bulk weight (γ), slope height (m)
6	0.181	0.262	1	2.5	Cohesion (c), friction angle (α)
7	0.236	0.461	3	7.5	Cohesion (c), slope angle (β)
8	0.191	0.342	5	12.5	Cohesion (c), slope height (H)
9	0.408	0.872	5	12.5	Friction angle (α), pore pressure ratio (Ru)
10	0.187	0.211	2	5	Slope angle (β), slope height (H)
11	0.395	1.427	4	10	Slope angle (β), pore pressure ratio (Ru)

and MARS model. BPNN and MARS models can model the relationship between the safety factor and the slope parameters. In this data set, the correlation coefficient R^2 in the BPNN model is 0.8931, and the value in the MARS model is 0.8629. However, the training time of the BPNN model is 95.61 s, whereas that of the MARS model is 8.63 s. The BPNN model will spend more time to train the model and obtain a predicted safety factor, and the precision of which is slightly bigger than that of the MARS model.

5.2 Parameter relative importance

After the MARS model is built; all the involved BFs are grouped based on the analysis of variance (ANOVA) decomposition [27]. This procedure is used to assess the contributions of the six influencing factors of slope stability. Table 2 presents the ANOVA decomposition, which is obtained by using the MARS model. The last column provides the particular input variable associated with the ANOVA function. Based on the information, the relative importance of the input influence factors of slope stability for the MARS model is evaluated based on the increase in the GCV and STD values. All the conditioning factors have contributed to the model; however, the slope angle is the most important one.

In the MARS model, the GCV and STD values of the slope angle are taken as the reference value. Figure 4 shows the comparison of the relative importance of the input variables based on the BPNN and MARS models. Compared with other parameters, the safety factor is more sensitive to slope height in the BPNN model. In the MARS model, the slope angle is the most sensitive parameter. The results indicate that the relative importance of

the input variables obtained by different machine learning models may vary. Nevertheless, all of these variables can predict the output value effectively.

5.3 Interpreted MARS model

Table 3 lists the BFs and their corresponding equation for the developed MARS model. Table 3 shows that interactions have occurred among BFs (25 of the 66 BFs are interaction terms). The presence of interactions suggests that the built MARS model is not simply additive, and interactions play a significant role in building an accurate model for capacity energy predictions. Without making any specific assumption about the underlying functional relationship between the input variables and the dependent response, MARS can capture the nonlinear and complex relationships between energy capacity and a multitude of initial geotechnical parameters with interactions
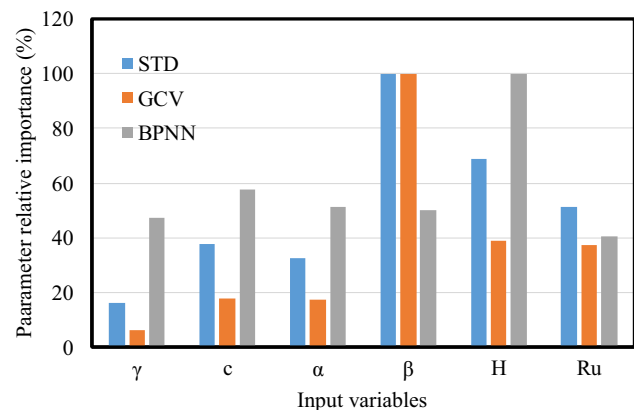
Figure 4: Relative importance of the input variables based on the BPNN and MARS models.

Table 3: Expressions of BFs for the developed MARS model

BF	Equation	BF	Equation
BF1	max(0, 50 −$x5$)	BF14	BF2 * max(0, 0.25 −$x6$)
BF2	max(0, 45.3 −$x4$)	BF15	max(0, 45.02 −$x2$) * max(0, $x5$ −37)
BF3	max(0, $x4$ −45.3) * max(0, 0.25 −$x6$)	BF16	BF5 * max(0, $x3$ −36)
BF4	max(0, $x5$ −50) * max(0, $x4$ −40.02)	BF17	max(0, 45.02 −$x2$) * max(0, $x4$ −40)
BF5	max(0, $x6$ −0.45)	BF18	max(0, 0.45 −$x6$) * max(0, 26.6 −$x3$)
BF6	max(0, 45.02 −$x2$) * max(0, $x1$ −20.41)	BF19	max(0, 45.02 −$x2$) * max(0, $x5$ −50)
BF7	max(0, 0.45 −$x6$) * max(0, 50 −$x4$)	BF20	max(0, 45.02 −$x2$) * max(0, 50 −$x5$)
BF8	max(0, 0.45 −$x6$) * max(0, $x3$ −22.01)	BF21	max(0, $x3$ −9.99) * max(0, 24.9 −$x2$)
BF9	max(0, 0.45 −$x6$) * max(0, 22.01 −$x3$)	BF22	max(0, $x3$ −9.99) * max(0, 0.25 −$x6$)
BF10	max(0, $x2$ −45.02) * max(0, $x5$ −120)	BF23	BF1 * max(0, $x1$ −16.47)
BF11	max(0, $x2$ −45.02) * max(0, 120 −$x5$)	BF24	max(0, 45.02 −$x2$) * max(0, $x4$ −22)
BF12	BF2 * max(0, $x5$ −115)	BF25	max(0, 45.02 −$x2$) * max(0, 22 −$x4$)
BF13	BF2 * max(0, $x6$ −0.25)		

among one another. The equation of MARS energy capacity model is given by

$$
\begin{aligned}
y = {}&1.24 + 0.017 \times \text{BF1} + 0.0545 \times \text{BF2} - 0.62 \\
&\times \text{BF3} - 0.00017 \times \text{BF4} + 5.18 \times \text{BF5} + 0.0015 \\
&\times \text{BF6} - 0.16 \times \text{BF7} + 0.23 \times \text{BF8} - 0.33 \times \text{BF9} \\
&- 6.87e - 05 \times \text{BF10} - 6.45e - 05 \times \text{BF11} \\
&- 0.00043 \times \text{BF12} - 0.30 \times \text{BF13} + 0.23 \\
&\times \text{BF14} - 0.0010 \times \text{BF15} + 3.83 \times \text{BF16} \\
&+ 0.0021 \times \text{BF17} + 0.23 \times \text{BF18} + 0.0011 \\
&\times \text{BF19} - 0.00024 \times \text{BF20} + 0.00088 \times \text{BF21} \\
&- 0.107 \times \text{BF22} - 0.0027 \times \text{BF23} - 0.0012 \\
&\times \text{BF24} - 0.0032 \times \text{BF25}
\end{aligned}
$$

In this section, the results of slope stability assessment based on BPNN and MARS are compared. Compared with BPNN, the MARS model is easy to be interpreted. Although the precision of the MARS model is slightly lower than that of the BPNN model, it will spend less time to train the model and obtain a predicted safety factor. In the monitoring and early warning of slope stability, the time factor is more important for people. Also, the MARS model can capture the intrinsic nonlinear and multidimensional relationship between the safety factor and the slope parameters.

6 Conclusions

This study explores the use of MARS to capture the intrinsic nonlinear and multidimensional relationship between the parameters, which is associated with the evaluation of slope stability. A comparative study of machine learning solutions for slope stability assessment that relied on BPNN and MARS was conducted. One data set with actual slope collapse events was utilized for model development and to compare the performance of BPNN and MARS. The results suggest that BPNN and MARS models can demonstrate the relationship between the safety factor and the slope parameters. Also, the MARS model has the advantage of computational efficiency and easy interpretation. The relative importance of the input variables obtained by different machine learning models may vary. Nevertheless, all of these variables can predict the output value effectively.

References

[1] Peruccacci S, Brunetti MT, Gariano SL, Melillo M, Rossi M, Guzzetti F. Rainfall thresholds for possible landslide occurrence in Italy. Geomorphology. 2017;290:39–57. doi: 10.1016/j.geomorph.2017.03.031.

[2] Wu DA, Bai JB, Wang XY, Yan S, Wu SX. Numerical study of failure mechanisms and control techniques for a gob-side yield pillar in the Sijiazhuang Coal Mine, China. Rock Mech Rock Eng. 2019a;52(4):1231–45. doi: 10.1007/s00603-018-1654-3.

[3] Wu DA, Bai JB, Wang XY, Zhu ZJ, Yan S. Field investigation of fractures evolution in overlying strata caused by extraction of the Jurassic and Carboniferous coal seams and its application: case study. Int J Coal Geol. 2019b;208:12–23. doi: 10.1016/j.coal.2019.04.002.

[4] Massey C, Pasqua FD, Holden C, Kaiser A, Richards L, Wartman J, et al. Rock slope response to strong earthquake

shaking. Landslides. 2016;14(1):1–20. doi: 10.1007/s10346-016-0684-8.

[5] Sun Y, Jiang Q, Yin T, Zhou C. A back-analysis method using an intelligent multi-objective optimization for predicting slope deformation induced by excavation. Eng Geol. 2018;239:214–28. doi: 10.1016/j.enggeo.2018.03.019.

[6] Li Q, Wang YM, Zhang KB, Yu H, Tao ZY. Field investigation and numerical study of a siltstone slope instability induced by excavation and rainfall. Landslides. 2020;17(6):1485–99. doi: 10.1007/s10346-020-01396-5.

[7] Zienkiewicz OC, Humpheson C, Lewis RW. Associated and non-associated visco-plasticity and plasticity in soil mechanics. Geotechnique. 1975;25(4):671–89. doi: 10.1680/geot.1975.25.4.671.

[8] Griffiths DV, Lane PA. Slope stability analysis by finite elements. Geotechnique. 1999;49(3):387–403. doi: 10.1680/geot.1999.49.3.387.

[9] Xu W, Wang S, Bilal M. LEM-DEM coupling for slope stability analysis. Sci China Technol Sci. 2020;63(2):329–40. doi: 10.1007/s11431-018-9387-2.

[10] Tschuchnigg F, Schweiger HF, Sloan SW, Lyamin AV, Raissakis I. Comparison of finite-element limit analysis and strength reduction techniques. Geotechnique. 2015;65(4):249–57. doi: 10.1680/geot.14.P.022.

[11] Reale C, Xue J, Gavin K. System reliability of slopes using multimodal optimisation. Geotechnique. 2016;66(5):413–23. doi: 10.1680/jgeot.15.P.142.

[12] Song DQ, Chen Z, Chao H, Ke YT, Nie W. Numerical study on seismic response of a rock slope with discontinuities based on the time-frequency joint analysis method. Soil Dyn Earthq Eng. 2020;133:106112. doi: 10.1016/j.soildyn.2020.106112.

[13] Jamalinia E, Vardon PJ, Steele-Dunne SC. The impact of evaporation induced cracks and precipitation on temporal slope stability. Comput Geotech. 2020;122:103506. doi: 10.1016/j.compgeo.2020.103506.

[14] Lee S, Ryu JH, Won JS, Park HJ. Determination and application of the weights for landslide susceptibility mapping using an artificial neural network. Eng Geol. 2004;71(3–4):289–302. doi: 10.1016/S0013-7952(03)00142-X.

[15] Wang HB, Xu WY, Xu RC. Slope stability evaluation using back propagation neural networks. Eng Geol. 2005;80(3–4):302–15. doi: 10.1016/j.enggeo.2005.06.005.

[16] Choobbasti AJ, Farrokhzad F, Barari A. Prediction of slope stability using artificial neural network (case study: Noabad, Mazandaran, Iran). Arab J Geosci. 2009;2(4):311–9. doi: 10.1007/s12517-009-0035-3.

[17] Conforti M, Pascale S, Robustelli G, Sdao F. Evaluation of prediction capability of the artificial neural networks for mapping landslide susceptibility in the Turbolo River catchment (northern Calabria, Italy). Catena. 2014;113:236–50. doi: 10.1016/j.catena.2013.08.006.

[18] Gordan B, Armaghani DJ, Hajihassani M, Monjezi M. Prediction of seismic slope stability through combination of particle swarm optimization and neural network. Eng Comput. 2016;32(1):85–97. doi: 10.1007/s00366-015-0400-7.

[19] Huang FM, Cao ZS, Guo JF, Jiang SH, Li S, Guo ZZ. Comparisons of heuristic, general statistical and machine learning models for landslide susceptibility prediction and mapping. Catena. 2020;191:104580. doi: 10.1016/j.catena.2020.104580.

[20] He S, Pan P, Dai L, Wang H, Liu J. Application of kernel-based Fisher discriminant analysis to map landslide susceptibility in the Qinggan River delta, Three Gorges, China. Geomorphology. 2012;171:30–41. doi: 10.1016/j.geomorph.2012.04.024.

[21] Ramos-Cañón AM, Prada-Sarmiento LF, Trujillo-Vela MG, Macías JP, Santos-r AC. Linear discriminant analysis to describe the relationship between rainfall and landslides in Bogotá. Colomb Landslides. 2016;13(4):671–81. doi: 10.1007/s10346-015-0593-2.

[22] Pham BT, Prakash I. Evaluation and comparison of LogitBoost Ensemble, Fisher's Linear Discriminant Analysis, logistic regression and support vector machines methods for landslide susceptibility mapping. Geocarto Int. 2019;34(3):316–33. doi: 10.1080/10106049.2017.1404141.

[23] Yeon YK, Han JG, Ryu KH. Landslide susceptibility mapping in Injae, Korea, using a decision tree. Eng Geol. 2010;116(3–4):274–83. doi: 10.1016/j.enggeo.2010.09.009.

[24] Bui DT, Pradhan B, Lofman O, Revhaug I. Landslide susceptibility assessment in Vietnam using support vector machines, decision tree, and Naive Bayes Models. Math Probl Eng. 2012;974638. doi: 10.1155/2012/974638.

[25] Pradhan B. A comparative study on the predictive ability of the decision tree, support vector machine and neuro-fuzzy models in landslide susceptibility mapping using GIS. Comput Geosci. 2013;51:350–65. doi: 10.1016/j.cageo.2012.08.023.

[26] Pourghasemi H, Pradhan B, Gokceoglu C, Moezzi KD. A comparative assessment of prediction capabilities of Dempster–Shafer and weights-of-evidence models in landslide susceptibility mapping using GIS. Geomat Nat Haz Risk. 2013;4(2):93–118. doi: 10.1080/19475705.2012.662915.

[27] Friedman JH. Multivariate adaptive regression splines. Ann Stat. 1991;19(1):1–67. doi: 10.1214/aos/1176347963.

[28] Kostić S, Vasović N, Todorović K, Samčović A. Application of artificial neural networks for slope stability analysis in geotechnical practice. In: Neural Networks and Applications (NEUREL). IEEE; 13th Symposium on November 2016. p. 1–6.

[29] Wasserman PD. Neural computing: theory and practice. Van Nostrand Reinhold Co; 1989.

[30] Yu W, Cai JL, An FP. Slope displacement prediction model based on LMD and BP neural network. AMM. 2013;246:370–6. doi: 10.4028/www.scientific.net/amm.246-247.370.

[31] Xu K, Guo Q, Li Z, Xiao J, Qin Y, Chen D, et al. Landslide susceptibility evaluation based on BPNN and GIS: A case of Guojiaba in the Three Gorges Reservoir Area. Int J Geogr Inf Sci. 2015;29(7):1111–24. doi: 10.1080/13658816.2014.992436.

[32] Demuth H, Beale M. Matlab neural network toolbox user's guide version 6. The MathWorks Inc.; 2009.

[33] Chen HQ, Zeng ZG. Deformation prediction of landslide based on improved back-propagation neural network. Cogn Comput. 2013;5(1):56–62. doi: 10.1007/s12559-012-9148-1.

[34] Erdik T, Pektas AO. Rock slope damage level prediction by using multivariate adaptive regression splines (MARS). Neural Comput Applic. 2019;31:2269–78. doi: 10.1007/s00521-017-3186-2.

[35] Sah NK, Sheorey PR, Upadhyaya LN. Maximum likelihood estimation of slope stability. Int J Rock Mech Min Abstr. 1994;31(1):47–53. doi: 10.1016/0148-9062(94)92314-0.

[36] Lu P, Rosenbaum MS. Artificial neural networks and grey systems for the prediction of slope stability. Nat Hazards. 2003;30(3):383–98. doi: 10.1023/B:NHAZ.0000007168.00673.27.

[37] Sakellariou MG, Ferentinou MD. A study of slope stability prediction using neural networks. Geotech Geol Eng. 2005;23(4):419. doi: 10.1007/s10706-004-8680-5.

[38] Li J, Wang F. Study on the forecasting models of slope stability under data mining. In: Earth and Space 2010: Engineering, Science, Construction, and Operations in Challenging Environments; 2010. p. 765–76. doi: 10.1061/41096(366)77.

[39] Manouchehrian A, Gholamnejad J, Sharifzadeh M. Development of a model for analysis of slope stability for circular mode failure using genetic algorithm. Environ Earth Sci. 2014;71(3):1267–77. doi: 10.1007/s12665-013-2576-8.

[40] Jekabsons G. ARESLab Adaptive Regression Splines toolbox for Matlab/Octave. Ver. 1.13. 0. Riga Technical University; 2016.

[41] Hoang ND, Pham AD. Hybrid artificial intelligence approach based on metaheuristic and machine learning for slope stability assessment: a multinational data analysis. Expert Syst Appl. 2016;46:60–8. doi: 10.1016/j.eswa.2015.10.020.

Appendix: dataset used in this study

Table A1: Dataset used in this study (from ref. [35–39,41])

No.	Unit weight/γ (kN/m³)	Cohesion/c (kPa)	Friction angle/α (°)	Slope angle/β (°)	Slope height/H (m)	Pore pressure ratio/Ru	Safety factor /FS
1	18.68	26.34	15	35	8.23	0	1.11
2	16.5	11.49	0	30	3.66	0	1
3	18.84	14.36	25	20	30.5	0	1.875
4	18.84	57.46	20	20	30.5	0	2.045
5	28.44	29.42	35	35	100	0	1.78
6	28.44	39.23	38	35	100	0	1.99
7	20.6	16.28	26.5	30	40	0	1.25
8	14.8	0	17	20	50	0	1.13
9	14	11.97	26	30	88	0	1.02
10	25	120	45	53	120	0	1.3
11	26	150.05	45	50	200	0	1.2
12	18.5	25	0	30	6	0	1.09
13	18.5	12	0	30	6	0	0.78
14	22.4	10	35	30	10	0	2
15	21.4	10	30.34	30	20	0	1.7
16	22	20	36	45	50	0	1.02
17	22	0	36	45	50	0	0.89
18	12	0	30	35	4	0	1.46
19	12	0	30	45	8	0	0.8
20	12	0	30	35	4	0	1.44
21	12	0	30	45	8	0	1.86
22	23.47	0	32	37	214	0	1.08
23	16	70	20	40	115	0	1.1
24	20.41	24.9	13	22	10.67	0.35	1.4
25	19.63	11.97	20	22	12.19	0.41	1.35
26	21.82	8.62	32	28	12.8	0.49	1.03
27	20.41	33.52	11	16	45.72	0.2	1.28
28	18.84	15.32	30	25	10.67	0.38	1.63
29	18.84	0	20	20	7.62	0.45	1.05
30	21.43	0	20	20	61	0.5	1.03
31	19.06	11.71	28	35	21	0.11	1.09
32	18.84	14.36	25	20	30.5	0.45	1.11
33	21.51	6.94	30	31	76.81	0.38	1.01
34	14	11.97	26	30	88	0.45	0.625
35	18	24	30.15	45	20	0.12	1.12
36	23	0	20	20	100	0.3	1.2
37	22.4	100	45	45	15	0.25	1.8
38	22.4	10	35	45	10	0.4	0.9
39	20	20	36	45	50	0.25	0.96
40	20	20	36	45	50	0.5	0.83
41	20	0	36	45	50	0.25	0.79
42	20	0	36	45	50	0.5	0.67
43	22	0	40	33	8	0.35	1.45
44	24	0	40	33	8	0.3	1.58
45	20	0	24.5	20	8	0.35	1.37
46	18	5	30	20	8	0.3	2.05
47	26.49	150	33	45	73	0.15	1.23
48	26.7	150	33	50	130	0.25	1.8
49	26.89	150	33	52	120	0.25	1.8
50	26.57	300	38.7	45.3	80	0.15	1.18
51	26.78	300	38.7	54	155	0.25	1.2
52	26.81	200	35	58	138	0.25	1.2

Table A1: Continued

No.	Unit weight/γ (kN/m^3)	Cohesion/c (kPa)	Friction angle/α (°)	Slope angle/β (°)	Slope height/H (m)	Pore pressure ratio/Ru	Safety factor /FS
53	26.43	50	26.6	40	92.2	0.15	1.25
54	26.7	50	26.6	50	170	0.25	1.25
55	26.8	60	28.8	59	108	0.25	1.25
56	22.4	10	35	45	10	0.4	0.9
57	20	20	36	45	50	0.5	0.83
58	20	0	36	45	50	0.25	0.79
59	20	0	36	45	50	0.5	0.67
60	22	0	40	33	8	0.35	1.45
61	24	0	40	33	8	0.3	1.58
62	20	0	24.5	20	8	0.35	1.37
63	18	5	30	20	8	0.3	2.05
64	27	40	35	43	420	0.25	1.15
65	27	50	40	42	407	0.25	1.44
66	27	35	35	42	359	0.25	1.27
67	27	37.5	35	37.8	320	0.25	1.24
68	27	32	33	42.6	301	0.25	1.16
69	27	32	33	42.4	289	0.25	1.3
70	27.3	14	31	41	110	0.25	1.249
71	27.3	31.5	29.7	41	135	0.25	1.245
72	27.3	16.8	28	50	90.5	0.25	1.252
73	27.3	26	31	50	92	0.25	1.246
74	27.3	10	39	41	511	0.25	1.434
75	27.3	10	39	40	470	0.25	1.418
76	25	46	35	47	443	0.25	1.28
77	25	46	35	44	435	0.25	1.37
78	25	46	35	46	432	0.25	1.23
79	26	150	45	30	200	0.25	1.2
80	18.5	25	0	30	6	0.25	1.09
81	18.5	12	0	30	6	0.25	0.78
82	22.4	10	35	30	10	0.25	2
83	21.4	10	30.34	30	20	0.25	1.7
84	22	20	36	45	50	0.25	1.02
85	22	0	36	45	50	0.25	0.89
86	12	0	30	45	4	0.25	1.46
87	12	0	30	45	8	0.25	0.8
88	12	0	30	45	4	0.25	1.44
89	31.3	68	37	49	200.5	0.25	1.2
90	20	20	36	45	50	0.25	0.96
91	27	40	35	47.1	292	0.25	1.15
92	25	46	35	50	284	0.25	1.34
93	31.3	68	37	46	366	0.25	1.2
94	25	46	36	44.5	299	0.25	1.55
95	27.3	10	39	40	480	0.25	1.45
96	25	46	35	46	393	0.25	1.31
97	25	48	40	49	330	0.25	1.49
98	31.3	68.6	37	47	305	0.25	1.2
99	25	55	36	45.5	299	0.25	1.52
100	31.3	68	37	47	213	0.25	1.2
101	28.4	150.05	45	53	200	0.5	2.31
102	18.66	26.41	14.99	34.98	8.2	0	1.11
103	28.4	29.41	35.01	34.98	100	0	1.78
104	25.96	150.05	45	49.98	200	0	1.2
105	18.46	25.06	0	30	6	0	1.09
106	21.36	10.05	30.33	30	20	0	1.7
107	15.99	70.07	19.98	40.02	115	0	1.11

Table A1: Continued

No.	Unit weight/γ (kN/m³)	Cohesion/c (kPa)	Friction angle/α (°)	Slope angle/β (°)	Slope height/H (m)	Pore pressure ratio/Ru	Safety factor /FS
108	20.39	24.91	13.01	22	10.6	0.35	1.4
109	19.6	12	19.98	22	12.2	0.41	1.35
110	21.78	8.55	32	27.98	12.8	0.49	1.03
111	20.39	33.46	10.98	16.01	45.8	0.2	1.28
112	19.03	11.7	27.99	34.98	21	0.11	1.09
113	17.98	4.95	30.02	19.98	8	0.3	2.05
114	20.96	19.96	40.01	40.02	12	0	1.84
115	20.96	34.96	27.99	40.02	12	0.5	1.43
116	19.97	10.05	28.98	34.03	6	0.3	1.34
117	18.77	30.01	9.99	25.02	50	0.1	1.4
118	18.77	30.01	19.98	30	50	0.1	1.46
119	18.77	25.06	19.98	30	50	0.2	1.21
120	20.56	16.21	26.51	30	40	0	1.25
121	16.47	11.55	0	30	3.6	0	1
122	18.8	14.4	25.02	19.98	30.6	0	1.88
123	18.8	57.47	19.98	19.98	30.6	0	2.04
124	28.4	39.16	37.98	34.98	100	0	1.99
125	13.97	12	26.01	30	88	0	1.02
126	24.96	120.04	45	53	120	0	1.3
127	18.46	12	0	30	6	0	0.78
128	22.38	10.05	35.01	30	10	0	2
129	21.98	19.96	36	45	50	0	1.02
130	18.8	15.31	30.02	25.02	10.6	0.38	1.63
131	18.8	14.4	25.02	19.98	30.6	0.45	1.11
132	21.47	6.9	30.02	31.01	76.8	0.38	1.01
133	13.97	12	26.01	30	88	0.45	0.63
134	17.98	24.01	30.15	45	20	0.12	1.12
135	22.38	99.93	45	45	15	0.25	1.8
136	22.38	10.05	35.01	45	10	0.4	0.9
137	19.97	19.96	36	45	50	0.25	0.96
138	19.97	19.96	36	45	50	0.5	0.83
139	20.96	45.02	25.02	49.03	12	0.3	1.53
140	20.96	30.01	35.01	40.02	12	0.4	1.49
141	19.97	40.06	30.02	30	15	0.3	1.84
142	17.98	45.02	25.02	25.02	14	0.3	2.09
143	18.97	30.01	35.01	34.98	11	0.2	2
144	19.97	40.06	40.01	40.02	10	0.2	2.31
145	18.83	24.76	21.29	29.2	37	0.5	1.07
146	18.83	10.35	21.29	34.03	37	0.3	1.29
147	18.77	25.06	9.99	25.02	50	0.2	1.18
148	18.77	19.96	9.99	25.02	50	0.3	0.97
149	19.08	10.05	9.99	25.02	50	0.4	0.65
150	18.77	19.96	19.98	30	50	0.3	1
151	19.08	10.05	19.98	30	50	0.4	0.65
152	21.98	19.96	22.01	19.98	180	0	1.12
153	21.98	19.96	22.01	19.98	180	0.1	0.99